INTERNATIONAL JOURNAL OF OPTIMIZATION IN CIVIL ENGINEERING
Int. J. Optim. Civil Eng., 2019; 9(4):671-687

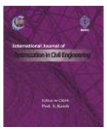

SEISMIC OPTIMIZATION OF STEEL SHEAR WALL USING SHAPE MEMORY ALLOY

R. Kamgar[1*, †], Y. Askari Dolatabad[2] and M. R. Babadaei Samani[3]
[1]*Department of Civil Engineering, Shahrekord University, Shahrekord, Iran*
[2]*Department of Civil Engineering, Sirjan University of Technology, Sirjan, Iran*
[3]*Department of Civil Engineering, Seed of Arian Saze Zagros, Chaharmahal Science & Technology Park, Shahrekord, Iran*

ABSTRACT

Nowadays, steel shear walls are used as efficient lateral-load-resistant systems due to their high lateral stiffness and carrying capacity. In this paper, the effect of substituting a shape memory alloy (SMA) material is investigated instead of using conventional steel in the shear wall. A numerical study is conducted using finite element method (FEM) by OpenSees software. For this purpose, at first, to verify the numerical simulation, the results of the experimental data are compared with those obtained from the numerical phase. Finally, the behavior of a one-bay three-story steel frame equipped with shear walls made of conventional steel, shape memory alloy and a combination of these two materials are studied when the structure is subjected to cyclic and seismic loadings. Results indicate that the use of shape memory alloy increases the maximum deformation, the yield displacement, and also the loading capacity of the structure. Also, it decreases the residual deformation of the structure and its initial stiffness. In general, using composite materials of conventional steel and shape memory alloy can reduce the maximum value of compression axial load of the column and, as a result, increase maximum rotation at the connections. In addition, the minimum and maximum values of base shear occurred in the model with 50% and 25% of Ni-Ti SMA material, respectively.

Keywords: shear wall; shape memory alloy; cyclic loading; seismic loading; strip method.

Received: 20 February 2019; Accepted: 15 July 2019

1. INTRODUCTION

Nowadays, shear walls are widely used as an efficient system in resisting the lateral load [1-

[*]Corresponding author: Department of Civil Engineering, Shahrekord University, Shahrekord, Iran
[†]E-mail address: kamgar@sku.ac.ir (R. Kamgar)

6]. This system has the ability to provide lateral stiffness and high load carrying capacity, especially in tall structures [1]. Also, there are numerous studies in the field of optimization to optimize and predict engineering problems [7-14]. Results of a research conducted by Gou and his colleagues showed that structures with steel shear wall (SSW) exhibited strong resistance during a severe earthquake [15]. Shao *et al.* used the capacity spectrum method to evaluate the seismic performance of a steel frame with a shear wall. In their study, the steel frame structure was retrofitted with a shear wall, which was designed according to the requirements of China design regulations. The base shear vs. top displacement curve of the frame was considered to construct the capacity spectrum for a single degree of freedom system [16]. Cao *et al*. performed a quasi-dynamic test on the steel frame retrofitted with SSW in order to investigate the seismic performance of this system. The structure was a one-bay, three-story building, which was studied when subjected to four earthquakes. Findings of their study revealed that the beam-to-shear wall connection caused lateral stiffness, energy dissipation capacity and sufficient resistance against the lateral load, due to the creation of the tension field action [17].

Also, SSW is considered important by many engineers for its significant features, including high ability to absorb energy, stable cyclic behavior and high deformation capacity. However, if the shear buckling occurs in early stages of behavior, the out-of-plane deformation occurred by plate buckling reduces its efficiency against mild and moderate earthquakes [18]. To overcome this defect, two major methods have been proposed, including the addition of stiffeners to the SSW and use of materials with a low yield point [18]. Haddad *et al*. investigated SSWs with a variety of circular and transverse stiffeners and concluded that the shear stiffness, ductility, and energy absorption of specimens with stiffeners increased [19]. Huang *et al.* proposed a new system of composite shear walls in which two steel plate were used around a concrete layer, with cross stiffeners between the steel plates. The results of their study showed that this system had a high ability to provide more ductility and energy absorption [20].

Also, several studies have been carried out on the shear wall using new materials replaced with conventional steel. An experimental study on the stiffened aluminum shear wall has been done by Matteis *et al.* They indicated that the energy absorption capacity increased due to the low yield point of this material [21]. Also, the results of a research carried out on the behavior of a shear wall with low-yield point steel material by Shahi and Adibrad indicated an increase in bearing capacity in comparison with the shear wall made of conventional steel material [22]. Zhang *et al.* proposed a buckling resistance steel shear system, in which low yield point steel was used in the construction of the shear wall. In this system, to prevent the initial buckling, there were stiffeners in the shear wall. They found that the buckling of the shear wall appeared at higher levels in this new system, which reduces the maximum structural drift [18].

According to the findings of the above-mentioned studies, reducing the residual deformation of the shear wall, occurred by the buckling of the plate, increases its efficiency in energy absorbing and providing the required ductility of the structure in the face of the seismic loads. In this paper, the shape memory alloy (SMA) material are replaced with the conventional steel in the construction of shear wall plate and a numerical study is conducted on the effect of replacing steel material with SMA material using finite element method by OpenSees software [23]. For this purpose, at first, a three-story steel frame with SSW is

modeled and the numerical results are compared with the experimental results. It is shown that the numerical method has been able to predict the structural responses in comparison with the experimental method. Then, the behavior of an SMA bar under cyclic loading is verified by OpenSees software in comparison with the experimental results. Verification results reveal the high accuracy of numerical methods in the prediction of structural behavior. Finally, the behavior of the three-story steel frame with a steel and SMA shear wall under cyclic and seismic loading is investigated. Also, the behavior of steel frame with the shear wall made of combined materials (a combination of SMA and ordinary steel in cross section of shear wall) is studied to evaluate its benefits under seismic loading. It is indicated that the use of shape memory alloy increases the maximum deformation of the structure, the yield displacement of the structure and also the bearing capacity of the structure. It also decreases the residual deformation of the structure and initial stiffness of the structure. In addition, the use of this material has been able to reduce the maximum value of the axial force of the columns. The use of composite materials of conventional steel and shape memory alloy can reduce the maximum value of compression axial load of the column. By increasing the percentage of shape memory alloy used in the construction of the shear wall up to α =0.25, the energy absorption capacity in the shear wall is increased and with increasing this percentage (α), the energy absorption capacity decreases in the shear wall.

2. SHAPE MEMORY ALLOY (SMA) MATERIAL

Today, a large part of researches in the field of civil engineering has been concentrated on the rehabilitation of structures against earthquakes. Increasing the load capacity, ductility, and energy absorption in the face of dynamic forces, as well as reducing structural damages are the main factors in the formation of new methods and the use of new materials. Regarding the use of FRP laminates and low yield point (LYP) steel in the main structural elements (directly or to retrofit the structural members), it can be observed that recent researches have attracted their attention to the use of super elastic shape memory alloy materials [24].

The SMA is a kind of alloy steel that has the ability to return to its original state after suffering from large deformations. For these materials, the reversibility to the initial state can occur by heat or removal of stress, which represents the shape memory effect and the super elastic property of them, respectively. The stress-strain curve of SMA material is shown in Figure 1. The stress-strain curve of the SMA material: a) Experimental result, b) Numerical model [25]. As can be seen, if loading takes place in any state, no residual stresses would remain in the material. Also, the SMA has a completely different set of mechanical properties than that of the conventional steel material. For example, the nickel-titanium shape memory alloy (Ni-Ti SMA) material has a density of 6.45 g/cm^3 (17% lighter than conventional steel) and a modulus of elasticity of 30-83 GPa (2.41 times less than conventional steel) and the ability to return to the initial state after experiencing over 8% strain [26].

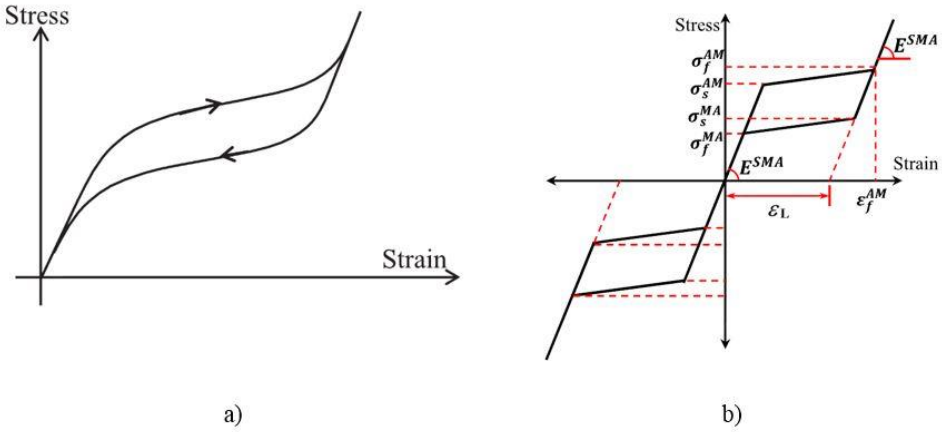

Figure 1. The stress-strain curve of the SMA material: a) Experimental result, b) Numerical model [25]

Various studies have been conducted on the use of these materials. Andrawes and Shin examined the use of Ni-Ti SMA in the spiral reinforcement for the reinforced concrete columns of the bridge as the active confinement. The results of this research showed that the use of these types of confinements reduced the maximum structural drift as compared with the FRP laminates [27]. Also, this material can be used to apply the controlled pre-stressing on the structural elements [28]. Using shape memory property of this material, Izadi *et al.* used iron-based SMA for the aim of investigating the effect of pre-stressing the steel plat. The results of this research made it clear that the pre-stress applied to the steel plate increased its yield stress and resistance to fatigue [29].

3. NUMERICAL MODELING

3.1 Modeling of steel frame with SSW

This section is devoted to represent a verification of the experimental results with the numerical results. For this purpose, the experimental specimen investigated by Park *et al.* [30] is modeled employing the finite element method in OpenSees software. As shown in Fig. 2, the model is a one-bay three-story steel frame with SSW. Other dimensions and specifications used for the modeling are presented in Table 1.

Table 1: The used properties of the elements for the studied model

Element		Dimensions (mm)				F_y	F_u
		h	b_f	t_w	t_f	(MPa)	(MPa)
Beams	Storey 1 & 2	200	200	16	16	330	600
	Storey 3	400	400	16	16		

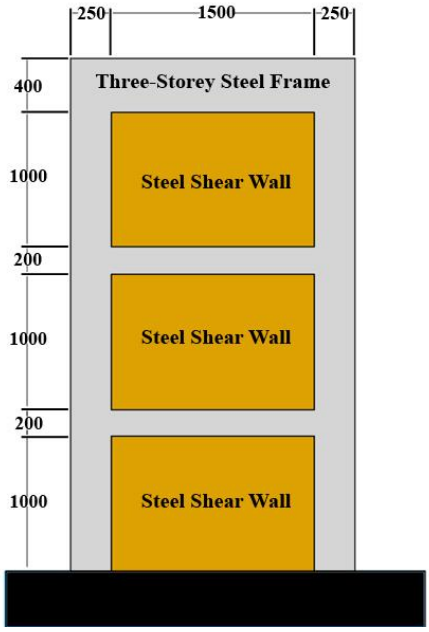

Figure 2. Details of the studied model

The nonlinearBeamColumn element is used to model the elements of the steel frame (beams and columns) which can investigate the nonlinear deformations. Also, the SSW is modeled using the strip method described in [31]. In this method, the SSW is replaced with a number of diagonal elements as shown in Fig. 3. These diagonal strips are pinned to the boundary frame in two directions and can simulate the behavior of the SSW. The area (A_s) and the angle (α) of each strip are calculated by Eqs. (1) and (2), respectively.

$$A_s = \frac{[L\cos\alpha + h\sin\alpha]t}{n} \quad [32] \quad (1)$$

$$\alpha = \tan^{-1}\sqrt{\frac{1+\frac{tL}{2A_c}}{1+th(\frac{1}{A_b}+\frac{h^3}{360I_cL})}} \quad [32] \quad (2)$$

where L, h, and t are the length, height and the thickness of the SSW. Also, A_c and I_c are the area and the moment of inertia of the boundary columns. A_b is the area of beams and n shows the number of strips. These strips are modeled using the truss element in the OpenSees software.

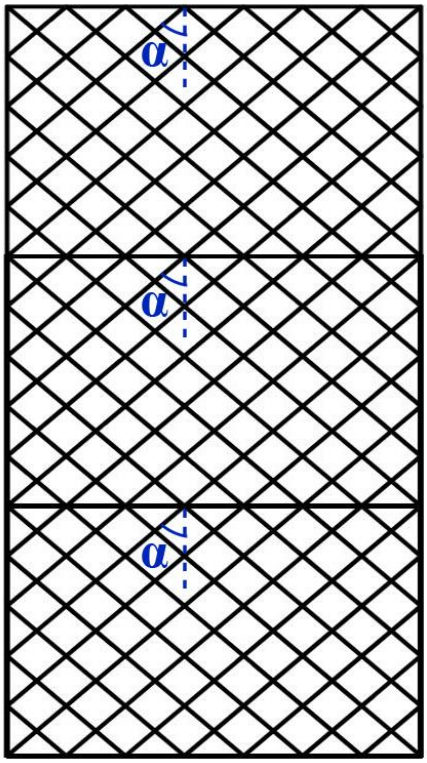

Figure 3. Strip method for the SSW modeling

Also, the hysteretic behavior model is used to model the mechanical behavior of steel in cyclic loading (Fig. 4). It is noteworthy that the cyclic loadings act as numbers of coefficients of yield displacement of the steel frame applied to the left of the upper beam, as illustrated in Fig. 5.

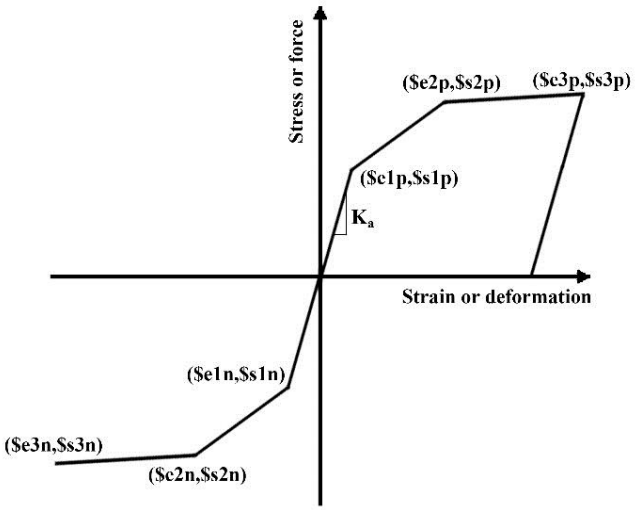

Figure 4. Steel behavior model [23]

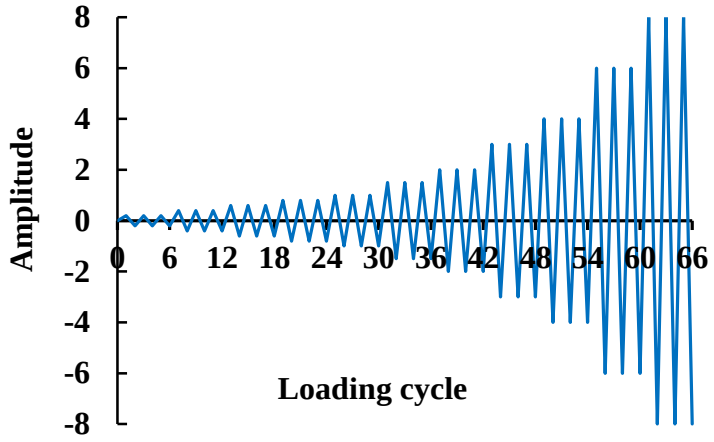

Figure 5. The used cyclic loading [30]

The verification of the numerical and experimental results of the steel shear wall with SSW is shown in Fig. 6. The proposed load-displacement curve shows the displacement values of the cyclic loading point against the support reactions. According to the obtained results, the numerical model can well simulate the behavior of the steel frame with SSW under cyclic loading. Table 2 shows the maximum value of the difference between the numerical and the experimental results. Based on the small differences between the experimental and numerical results, the numerical method has high ability to predict the structural behavior.

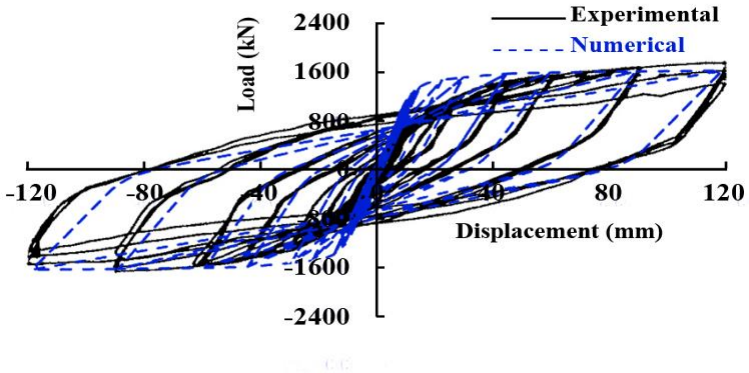

Figure 6. The load-displacement curve of the steel frame equipped with SSW

Table 2: The difference between the numerical and experimental results

Region	Max difference between displacements (%)	Max difference between loads (%)
Positive	-3.65	-5.88
Negative	-3.65	-2.32

3.2 Modeling of SMA material

In order to verify numerical modeling for the behavior of SMA material, an experimental study, carried out by DesRoches *et al.* [26], is modeled in OpenSees software. This experiment involves applying cyclic load on a Ni-Ti SMA reinforcement with 25.4 mm diameter. In OpenSees, one side of the element was fully supported and the cyclic loading was applied to the other side. Also, to simulate the mechanical behavior of a Ni-Ti SMA, the SMA material model [33] was used in the OpenSees software (Fig. 7).

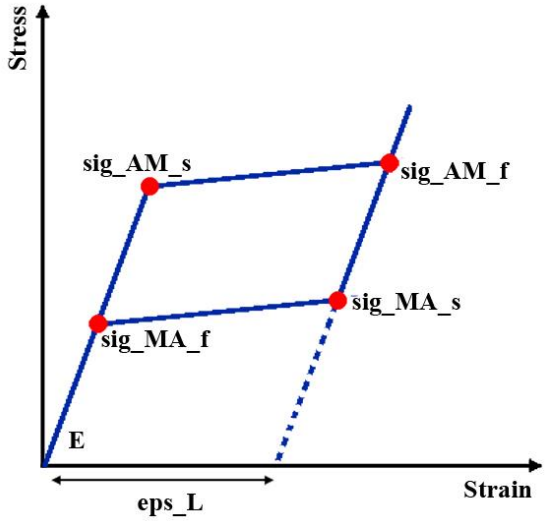

Figure 7. SMA behavior model [23]

Numerical analysis is performed to determine the accuracy of the modeling for Ni-Ti SMA. The required values for validation with the results of DesRoches *et al.* [26] are shown in Table 3. The stress-strain curve of numerical and experimental analysis is shown in Fig. 8. Table 4 shows the maximum value of the difference between the numerical and the experimental results. Based on the negligible difference between numerical and experimental results, the numerical method has a high ability to predict the behavior of the Ni-Ti SMA material.

Table 3: The parameters of SMA material

Parameter	Definition	Value
E	Modulus of elasticity for austenite	28 GPa
sig_AM_s	Austenite to martensite starting stress	372 MPa
sig_AM_f	Austenite to martensite finishing stress	570 MPa
sig_MA_s	Martensite to austenite starting stress	280 MPa
sig_MA_f	Martensite to austenite finishing stress	150 MPa
eps_L	Maximum residual strain (in martensite phase)	0.05

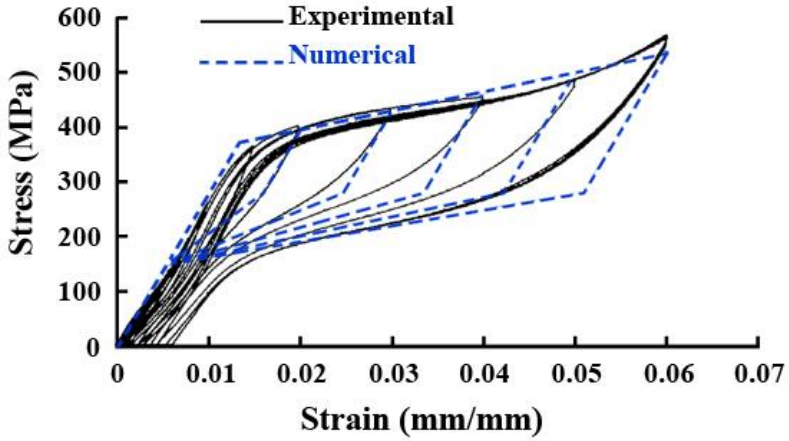

Figure 8. The stress-strain curve of numerical and experimental analyses

Table 4: Maximum difference between numerical and experimental results

The maximum difference between the strains (%)	The maximum difference between the stresses (%)
-0.009	-5.83

4. STUDYING THE EFFECTS OF USING SMA MATERIAL IN SHEAR WALL

4.1 Investigation of the cyclic behaviour

In this section, the behavior of the shear wall with two types of materials (conventional steel and Ni-Ti SMA) is investigated under cyclic loading (based on Fig. 5). In order to compare the results, ST-52 steel is used as SSW material which has a similar yield (F_y) and ultimate stress (F_u), when compared to the Ni-Ti SMA material. It should be noted that the initial and ultimate stresses of the martensite phase in a Ni-Ti SMA material are equal to 372 and 570 MPa, respectively. Also, for both of the considered shear walls (Steel and Ni-Ti SMA), the thickness of cross-section is equal to 2 mm (according to Eqs. 1 and 2).

The cyclic behavior of steel frame with two types of shear walls is shown in Fig. 9. Based on these curves, two important features can be observed for the steel frame with Ni-Ti SMA shear wall. Since the SMA material has a higher deformation capacity than the conventional steel, use of this material increases the deformation in the structure, as the maximum deformation in the steel frame with Ni-Ti SMA shear wall is 30.3% more than the steel frame with SSW. Considering the fact that, after a severe earthquake, common steel shear walls often suffer from residual deformations and that reusing them is not possible, use of SMA materials is recommended; because, there are no residual deformations after severe earthquakes. It should be noted that the visible deformation in Fig. 9 is a result of plastic deformation of structural members and, as in Fig. 8, there is no residual deformation in this material.

As mentioned previously, the super elastic property of the SMA material causes no residual deformation in this material. Therefore, this feature of SMA materials can be used to construct the structures that are to be used without interruption during and after the earthquake (Immediate Occupancy (IO) level).

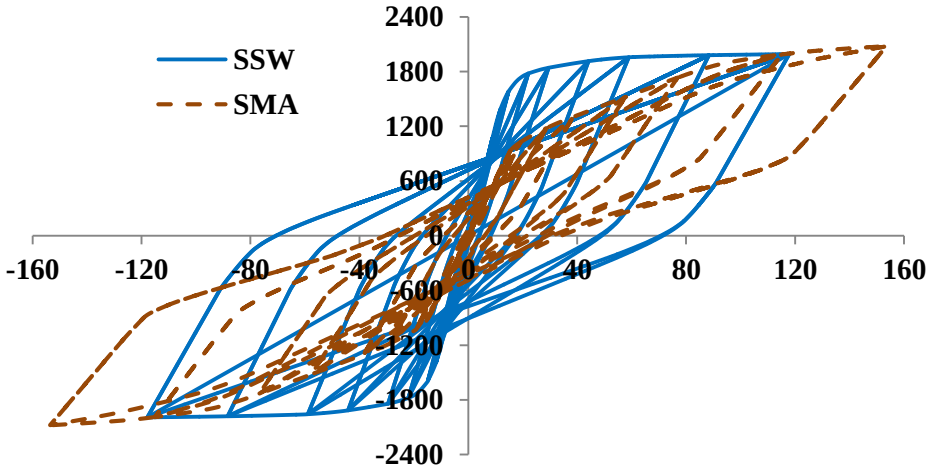

Figure 9. Cyclic behavior of steel frame with two types of shear walls

Table 5: Comparison of the results of using Ni-Ti SMA shear wall and SSW in the steel frame shows the comparison of the results of using Ni-Ti SMA shear wall and SSW in the steel frame. Accordingly, the Ni-Ti SMA shear wall increased the yield displacement by 30% and reduced the initial stiffness by approximately 50%; also, use of Ni-Ti SMA material increased the maximum displacement and the load capacity of the structure by 30, 4%, respectively. The only disadvantage of using these materials is the reduction of energy absorption by 19%. The reason for this reduction is the decrease of residual deformation by about 50% and this is one of the best advantages of using SMA materials.

Table 5: Comparison of the results of using Ni-Ti SMA shear wall and SSW in the steel frame

Shear Wall Material	Yield Disp. (*mm*)	Initial Stiffness (*kN/m*)	Max. Disp. (*mm*)	Max. Load (*kN*)	Energy Absorption (*kN.m*)	Negative Residual Disp. (*mm*)	Positive Residual Disp. (*mm*)
Steel (ST-52)	14.73	106458.7	117.84	1991.96	1633.58	-70	72
SMA Ni-Ti	19.2	52841.33	153.6	2079.68	1324.73	-30	35
Ratio of SMA to steel	1.30	0.496	1.30	1.04	0.81	0.4280	0.486

4.2 Investigation of the seismic behaviour

According to the results of the previous section, the use of any conventional steel and Ni-Ti SMA has its own advantages. Therefore, in this section, the shear wall with a combination of two ST-52 steel and Ni-Ti SMA is used to study the seismic behavior of the structure. For this purpose, five steel frames with combined (ST52 steel & Ni-Ti SMA) shear wall are

modeled, as details are shown in Table 6. Also, Takatori earthquake with characteristics described in Table 7, is selected for seismic analysis. For all the considered examples, the total thickness of the shear wall is 2 (*mm)*. In addition, based on Table 6, for example, SW-25 represents a cross-section for shear wall system that has 0.5 (*mm*) thickness for material with SMA property and 1.5 (*mm*) thickness for material with ST52 steel property. There are numerous time integration methods which can be used to solve the dynamic equations of motion for a structure subjected to the earthquake [34-36]. In this paper, the Newmark method is selected to solve the equations of motion.

Table 6: Details of models with combined shear wall

Model	The used value for Ni-Ti SMA (%)	Thickness of the shear wall (mm)	
		Ni-Ti SMA	Steel
SW-**0**	**0**	0.0	2.0
SW-**25**	**25**	0.5	1.5
SW-**50**	**50**	1.0	1.0
SW-**75**	**75**	1.5	0.5
SW-**100**	**100**	2.0	0.0

Table 7: Horizontal component characteristics of Takatori earthquake

PGA*(m/sec^2)	PGV* (m/sec)	Strong ground motion duration (sec)	Total time duration (sec)	Arias Intensity (m/sec)
6.052	0.665	11.85	40.96	6.34

*PGA: peak ground acceleration and PGV: peak ground velocity.

The values of the natural period, maximum values of roof displacement and also maximum values of base reaction are shown in Table 8. The maximum and minimum first natural period of the structure are accrued in SW-100 and SW-25, respectively. Also, Fig. 10 and Fig. 11 show the roof displacement and the base shear of the numerical models subjected to the Takatori earthquake, during the strong ground motion duration ($0 \le t \le 11.85$), respectively. The maximum displacement of the structure subjected to the earthquake has an incremental trend with adding the percentage of the Ni-Ti SMA material. The minimum values for base shear occur in SW-50 and also the maximum values occur in SW-25.

Table 8: Values of the first natural period, maximum roof displacement and maximum base shear for the studied models subjected to earthquake load

Model	T (*Sec*)	Max. Disp (*mm*)	Max. Base Reaction (*kN*)
SW-**0**	0.968	**338.6**	8247.5
SW-**25**	**0.862**	339.5	**8922.5**
SW-**50**	1.105	403.1	**8052.6**
SW-**75**	1.052	401.5	8399.6
SW-**100**	**1.382**	**482.5**	8260.9

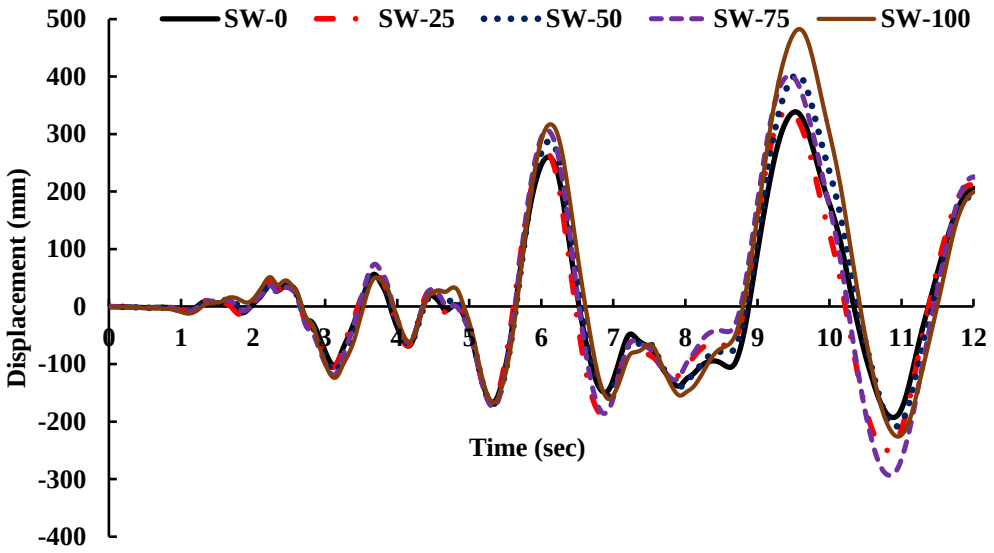

Figure 10. The time history of roof displacement for the steel frame subjected to earthquake

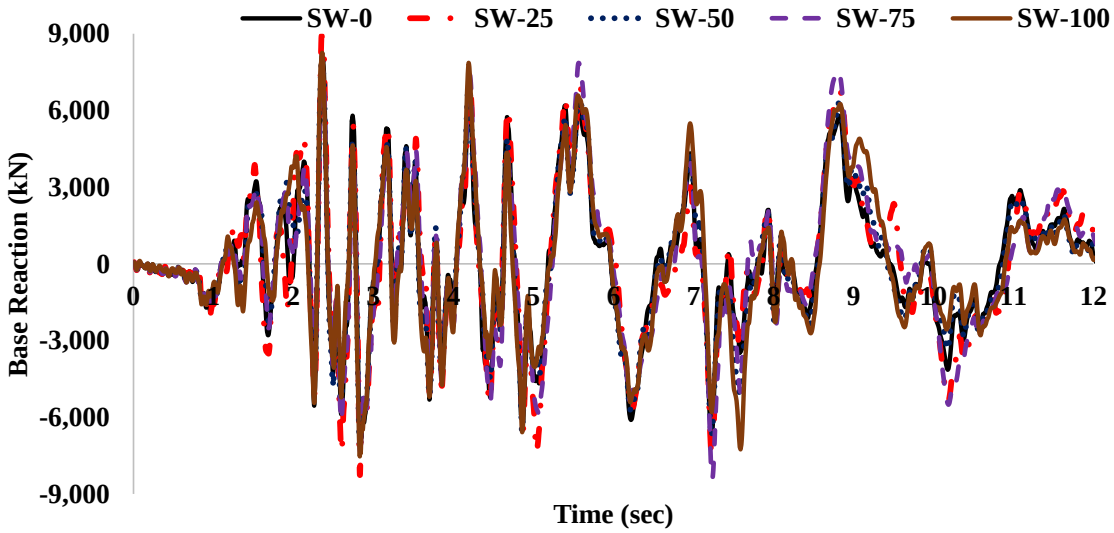

Figure 11. The time history of base shear for the steel frame subjected to the earthquake

In addition, the value for the axial load of the lowest left column of the steel frame is shown in Fig. 12. As can be seen, the compression load has a decreasing trend as the percentage of Ni-Ti SMA material increased; so it can help to prevent buckling of the column. Also, minimum tension load has occurred in the model with 50% of Ni-Ti SMA material (SW-50) and maximum tension load occurs in SW-25.

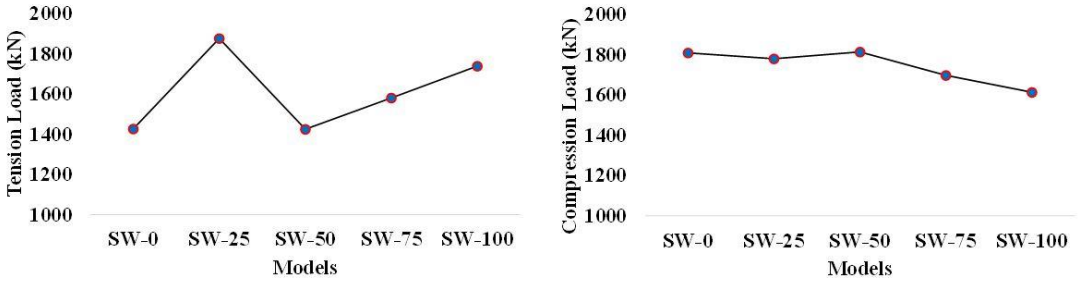

a) b)

Figure 12. A compression between the values of axial load in the lowest left column of the steel frame: a) tension load, b) compression load

The values of average shear distortion for the models are shown in Fig. 13. The average shear distortion can be calculated by Eq. (3) [37].

$$\gamma_{avg} = \frac{\sqrt{h_d^2 + l_d^2}\,(d_1 - d_2)}{2h_d l_d} \qquad [37] \qquad (3)$$

where h_d and l_d are the overall height and length of the models, respectively. Also d_1 and d_2 are the diagonal deformations. As shown in Fig. 13, the models with Ni-Ti SMA have greater values of the shear distortion. The maximum shear distortion has occurred for SW-100, where all of the shear walls of this model has made with Ni-Ti SMA material.

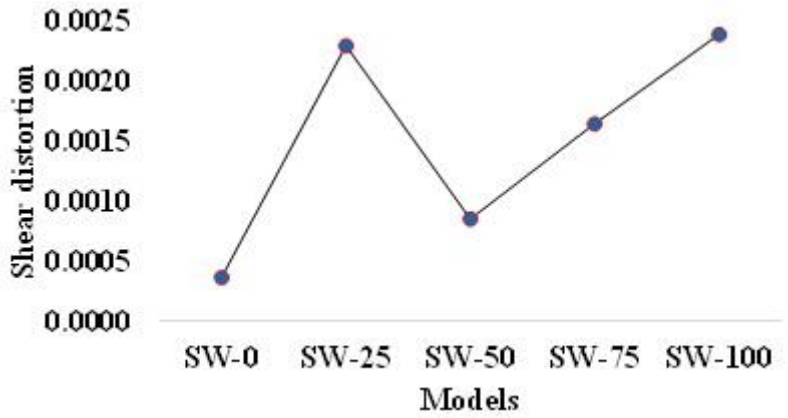

Figure 13. A comparison of average shear distortions of the studied models

Also, the rotation between the top left column and beam is shown in Fig. 14. Similar to the results of the previous section (average shear distortion), all of the models with Ni-Ti SMA material have greater rotation than the model without Ni-Ti SMA material. The maximum value for the rotation can be seen for SW-75.

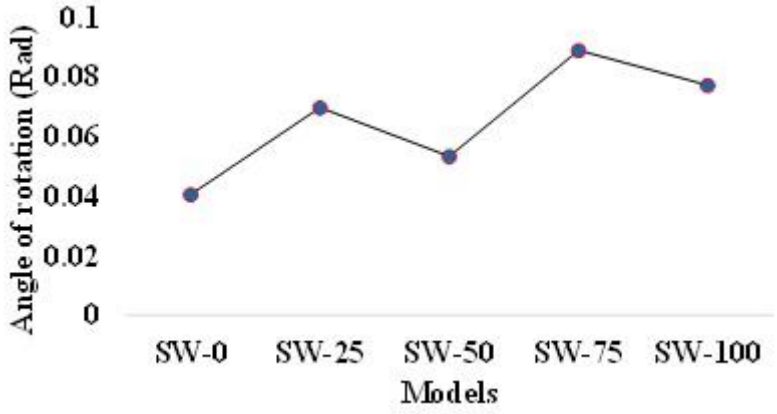

Figure 14. The angle of rotation for connection between the top left column and top beam

Finally, the values of energy absorption capacity of the shear wall are shown in Fig. 15. Based on this Figure, use of 25% Ni-Ti SMA material in the shear wall has a good effect in this field as the maximum value of the energy absorption has occurred in SW-25 which is greater than the model without Ni-Ti SMA material (SW-0). Also, the energy absorption capacity decreased by using more than 25% of Ni-Ti SMA material in the shear wall.

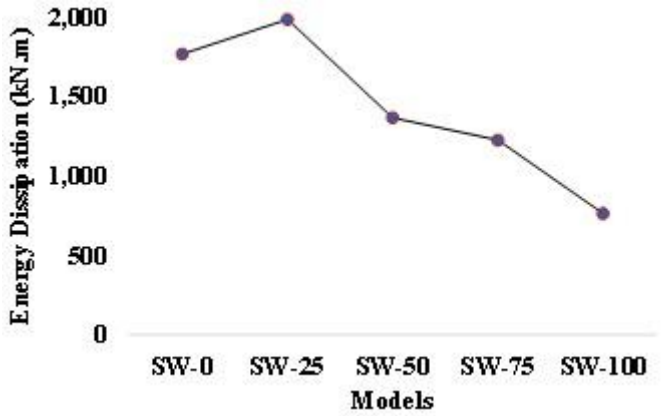

Figure 15. A comparison of the capacities of energy absorption

5. CONCLUSION

In this paper, the steel material in steel shear wall has been replaced by the shape memory alloy (SMA) material, and a numerical study has been carried out on the behavior of using SMA material by OpenSees software. For this purpose, a software model for a one-bay, three-story steel frame with steel shear wall is made and the results of the numerical analysis were verified against the experimental results. Then, the validation of the numerical modeling of Nickel-Titanium shape memory alloy (Ni-Ti SMA) material is conducted by experimental results. The verification results have made it obvious that the numerical model has a high ability to predict the behavior of the structure. Finally, the behavior of the steel

frame with a shear wall made of ST-52 steel and Ni-Ti SMA material has been investigated subjected to the cyclic and seismic loading. The results showed that:

1. Using Ni-Ti SMA material in the shear wall increases the deformation capacity of the structure by 30.3%.
2. Since the SMA material has no residual deformation after unloading, the residual deformation of the structure decreases by about 50% in the models with a shear wall which were fully made of Ni-Ti SMA material. So, this good ability can be used in the structures so as to be available during and after severe earthquakes.
3. Using Ni-Ti SMA material in shear wall decreased the yield displacement and the initial stiffness of the structure by 30% and 50%, respectively. Subsequently, the deformation capacity of the structure increased by 30%. Also, the load capacity of the structure increased by 4% in the model with Ni-Ti SMA material.
4. Ni-Ti SMA material decreased the energy absorption capacity by 19% because residual deformation of the structure and subsequently the area of the displacement-load curve decreased in the model where the shear wall was made of Ni-Ti SMA material.
5. Generally, there is an increasing trend for the first natural period of the structure with the use of Ni-Ti SMA material. So, the models with more Ni-Ti SMA material have lower stiffness. Also, the same results were observed for the deformation capacity where the structures with more Ni-Ti SMA material had greater values of deformation capacity.
6. The minimum base shear occurred in the model with 50% of Ni-Ti SMA material (SW-50). Furthermore, the maximum value occurred in SW-25. Also, similar results were obtained during the investigation of the tension load of columns, indicating the shear distortion of the structure and the rotation at the connection between the top left column and top beam. In addition, the values of the compression load of the lowest left column showed that increasing the Ni-Ti SMA material caused decreasing the compression load of columns. Therefore, it can be noted that shear wall made of 50% Ni-Ti SMA material presented better behavior in seismic loading.
7. The maximum energy dissipation of the shear wall occurred in the model with 25% of Ni-Ti SMA material, but the energy dissipation decreased with increasing the Ni-Ti SMA material from 25% to 100%. As previously mentioned, this was because of decreasing the residual deformation which caused decreases in the area of the load-displacement curve.

Acknowledgment: The authors would like to show their appreciations to HPC center (Shahr-e-Kord University, Iran) for their collaboration in offering computational clusters, which was a great help to complete this work.

REFERENCES

1. Kamgar R, Saadatpour MM. A simple mathematical model for free vibration analysis of combined system consisting of framed tube, shear core, belt truss and outrigger system with geometrical discontinuities, *Appl Mathemat Model* 2012; **36**(10): 4918-30.
2. Kaveh A, Farhadmanesh M. Optimal seismic design of steel plate shear walls using metaheuristic algorithms, *Period Polytech Civil Eng* 2019; **63**(1): 1-17.

3. Kaveh A, Zakian P. Performance based optimal seismic design of RC shear walls incorporating soil–structure interaction using css algorithm, *Int J Optim Civil Eng* 2012; **2**(3): 383-405.
4. Kaveh A, Zakian P. Optimal seismic design of reinforced concrete shear wall-frame structures, *KSCE J Civil Eng* 2014; **18**(7): 2181-90.
5. Kaveh A, Zakian P. Seismic design optimization of RC moment frames and dual shear wall-frame structures via CSS algorithm, *Asian J Civil Eng* 2014; **15**(3): 435-365.
6. Kaveh A, Zakian P. Topology optimization of shear wall structures under seismic loading, *Earthq Eng Eng Vibrat* 2018; **73**: 607-22.
7. Kamgar R, Khatibinia M, Khatibinia M. Optimization criteria for design of tuned mass dampers including soil-structure interaction effect, *Int J Optim Civil Eng* 2019; **9**(2): 213-32.
8. Kamgar R, Rahgozar P. Reducing static roof displacement and axial forces of columns in tall buildings based on obtaining the best locations for multi-rigid belt truss outrigger systems, *Asian J Civil Eng* 2019; **20**(6): 759-68.
9. Kamgar R, Rahgozar R. Determination of optimum location for flexible outrigger systems in non-uniform tall buildings using energy method, *Int J Optim Civil Eng* 2015; **5**(4): 433-44.
10. Kamgar R, Rahgozar R. Determination of optimum location for flexible outrigger systems in tall buildings with constant cross section consisting of framed tube, shear core, belt truss and outrigger system using energy method, *Int J Steel Struct* 2017; **17**(1): 1-8.
11. Kamgar R, Samea P, Khatibinia M. Optimizing parameters of tuned mass damper subjected to critical earthquake, *Struct Des Tall Special Build* 2018; **27**(7): e1460.
12. Kaveh A, Dadras Eslamlou A. An efficient two-stage method for optimal sensor placement using graph-theoretical partitioning and evolutionary algorithms, *Struct Control Health Monitor* 2019; **26**(4): e2325.
13. Kaveh A, Kabir M, Bohlool M. Optimum design of three-dimensional steel frames with prismatic and non-prismatic elements, *Eng Comput* 2019: 1-17.
14. Tavakoli R, Kamgar R, Rahgozar R. The best location of belt truss system in tall buildings using multiple criteria subjected to blast loading, *Civil Eng J* 2018; **4**(6): 1338-53.
15. Ge M, Hao J, Yu J, Yan P, Xu S. Shaking table test of buckling-restrained steel plate shear walls, *J Construct Steel Res* 2017; **137**: 254-61.
16. Shao Jh, Gu Q, Shen YK. Seismic performance evaluation of steel frame-steel plate shear walls system based on the capacity spectrum method, *J Zhejiang University-Science A* 2008; **9**(3): 322-9.
17. Cao ZG, Du P, Fan F, Chen ZM. Pseudo-dynamic testing of a fabricated composite frame with steel plate shear walls, *J Zhejiang University-Science A* 2017; **18**(6): 454-66.
18. Ma ZY, Hao JP, Yu HS. Shaking-table test of a novel buckling-restrained multi-stiffened low-yield-point steel plate shear wall, *J Construct Steel Res* 2018; **145**: 128-36.
19. Haddad O, Sulong N, Ibrahim Z. Cyclic performance of stiffened steel plate shear walls with various configurations of stiffeners, *J Vibroeng* 2018; **20**(1): 459-76.
20. Huang ST, Huang YS, He A, Tang XL, Chen QJ, Liu X, Cai J. Experimental study on seismic behaviour of an innovative composite shear wall, *J Construct Steel Res* 2018; **148**: 165-79.
21. De Matteis G, Mazzolani F, Panico S. Experimental tests on pure aluminium shear panels with welded stiffeners, *Eng Struct* 2008; **30**(6): 1734-44.

22. Shahi N, Adibrad M H. Finite-element analysis of steel shear walls with low-yield-point steel web plates, *Proceedings of the Institution of Civil Engineers, Structures and Buildings* 2017; **171**(4): pp. 326-337.
23. Mazzoni S, McKenna F, Scott MH, Fenves GL. OpenSees command language manual, in *Pacific Earthquake Engineering Research (PEER) Center*, 2006.
24. Parvin A, Raad J. Internal and external reinforcement of concrete members by use of shape memory alloy and fiber reinforced polymers under cyclic loading: a review, *Polymers* 2018; **10**(4): 376.
25. Abou-Elfath H. Evaluating the ductility characteristics of self-centering buckling-restrained shape memory alloy braces, *Smart Mater Struct* 2017; **26**(5): 055020.
26. DesRoches R, McCormick J, Delemont M. Cyclic properties of superelastic shape memory alloy wires and bars, *J Struct Eng* 2004; **130**(1): 38-46.
27. Andrawes B, Shin M. Seismic retrofitting of bridge columns using shape memory alloys, in *Active and Passive Smart Structures and Integrated Systems 2008*, International Society for Optics and Photonics, 2008
28. Rojob H, El-Hacha R. Self-prestressing using iron-based shape memory alloy for flexural strengthening of reinforced concrete beams, *ACI Struct J* 2017; **114**(2): 523.
29. Izadi M, Ghafoori E, Shahverdi M, Motavalli M, Maalek S. Development of an iron-based shape memory alloy (Fe-SMA) strengthening system for steel plates, *Eng Struct* 2018; **174**: 433-46.
30. Park HG, Kwack JH, Jeon SW, Kim WK, Choi IR. Framed steel plate wall behavior under cyclic lateral loading, *J Struct Eng* 2007; **133**(3): 378-88.
31. Sabelli R, Bruneau M. *Design Guide 20: Steel Plate Shear Walls*, American Institute of Steel Construction, Chicago, IL, USA, 2007.
32. Thorburn LJ, Montgomery C, Kulak GL. Analysis of Steel Plate Shear Walls, 1983.
33. Fugazza D. Shape-Memory Alloy Devices for Earthquake Engineering: Mechanical Properties, Constitutive Modeling and Numerical Simulations, Rose school, European school of advanced studies in reduction of seismic risk, 2003.
34. Kamgar R, Rahgozar R. A simple method for determining the response of linear dynamic systems, *Asian J Civil Eng* 2016; **17**(6): 785-801.
35. Rostami S, Shojaee S. Alpha-modification of cubic B-Spline direct time integration method, *Int Struct Stabil Dyn* 2017; **17**(10): 1750118.
36. Rostami S, Shojaee S. A family of cubic B-Spline direct integration algorithms with controllable numerical dissipation and dispersion for structural dynamics, *Iranian J Sci Technol, Transact Civil Eng* 2018; **42**(1): 17-32.
37. Choi IR, Park HG. Cyclic loading test for reinforced concrete frame with thin steel infill plate, *J Struct Eng* 2011; **137**(6): 654-64.